Proton Transfer in Perfluorosulfonic Acid Fuel Cell Membranes with Differing Pendant Chains and Equivalent Weights

Joseph E. Thomaz, Christian M. Lawler[+], and Michael D. Fayer*

Department of Chemistry
Stanford University, Stanford, CA 94305
*fayer@stanford.edu
650 723-4446

Abstract

Proton transfer in the nanoscopic water channels of polyelectrolyte fuel cell membranes was studied using a photoacid, 8-hydroxypyrene-1,3,6-trisulfonic acid sodium salt (HPTS) into the channels. The local environment of the probe was determined using 8-methoxypyrene-1,3,6-trisulfonic acid sodium salt (MPTS), which is not a photoacid. Three fully hydrated membranes, Nafion (DuPont) and two 3M membranes, were studied to determine the impact of different pendant chains and equivalent weights on proton transfer. Fluorescence anisotropy and excited state population decay data that characterize the local environment of the fluorescent probes and proton transfer dynamics were measured. The MPTS lifetime and anisotropy results show that most of the fluorescent probes have a bulk-like water environment with a relatively small fraction interacting with the channel wall. Measurements of the HPTS protonated and deprotonated fluorescent bands' population decays provided information on the proton transport dynamics. The decay of the protonated band from ~0.5 ns to tens of ns is in part determined by dissociation and recombination with the HPTS, providing information on the ability of protons to move in the channels. The dissociation and recombination is manifested as a power law component in the protonated band fluorescence decay. The results show that equivalent weight differences between two 3M membranes resulted in a small difference in proton transfer.

However, differences in pendant chain structure did significantly influence the proton transfer ability, with the 3M membranes displaying more facile transfer than Nafion.

[+]Permanent address: Lam Research Corporation, Fremont CA 94538

I. Introduction

Although the original concept was developed in 1839, fuel cells have only been used to meet specific energy needs since the 1960's.[1-2] When implemented on a large scale, such as for use on the space shuttle,[3] fuel cells have the capability to function at conversion levels of 50-60%.[4] Such high conversion levels, however, are not attained in products that would be used regularly in consumer markets.[5-7] One key component of fuel cells is the semipermeable proton exchange membrane.[8] As the electrolyte, these membranes lie in the center of the fuel cell, and allow charge to pass from the anode to the cathode. Efficient membranes improve fuel cell performance. In addition, membrane cost reduction is an important aspect for wide spread use of fuels, making the move toward a hydrogen economy more viable.[9-11]

The membrane that has been used most extensively is Nafion developed by DuPont. Nafion consists of a Teflon backbone with fluoropolymer pendant chains with strongly hydrophilic sulfonic acid head groups and hydrogen counterions. The hydrophobic nature of the backbones compared to the hydrophilic nature of the sulfonic acid head groups results in the formation of nanoscopic channels available for proton transfer.[12] These nanoscopic channels swell upon hydration providing paths for protons diffusion through the membrane. The water containing channels enable proton transport between electrodes during fuel cell operation. Nafion has been considered the industry standard since the late 1960's. More recently, 3M has developed new fuel cell membranes utilizing different perfluorosulfonic acid chains.[13] A comparison of the pendant chains is shown in Figure 1; the main differences are the absence of a tertiary trifluoromethyl group and an ether linkage in the 3M membranes that are present in the Nafion membranes. Molecular dynamics simulations suggest that the new 3M membranes may be able to transfer protons more efficiently than Nafion at room temperature.[14] It is desirable to

obtain experimental information on the effect of such polymer alterations on the fundamental dynamics of proton transfer in these membranes.

Previous experiments have characterized the channel structure of Nafion membrane; however there is still not a true consensus.[15-20] In the late 1970's and early 1980's Gierke and coworkers using small angle X-ray scattering (SAXS) experiments described the channels as a series of reverse micelle-like 4 nm pores connected by smaller 1 nm channels. However, since then it has been determined that it is likely that this model is incorrect.[21-22] More recent studies have described the system as being composed of irregular channels with nanometer length scale diameters.[12, 23-26] In this paper, we provide a comparison of proton transfer dynamics on mezoscopic distances scales and some information on the channel structure in the Nafion membrane and its 3M counterparts. Another variable found in membranes is the equivalent weight. Modifying the equivalent weight of a membrane has a direct effect on the pore of the membrane.[27] The equivalent weight is the molecular mass of a polymer segment that contains a single pendant chain with one sulfonate head group.[8] For this reason, two equivalent weights of 3M membranes were studied. Table 1 lists the membranes studied and their equivalent weights. Additionally, one must consider the hydration level, denoted as λ, of each membrane in order for comparisons to be made. More specifically, λ refers to the number of water molcules per sulfonate headgroups. In this case, the membranes saturated in water have nearly the same hydration level.

The photoacid 8-hydroxypyrene-1,3,6-trisulfonic acid sodium salt (HPTS) and 8-methoxypyrene-1,3,6-trisulfonic acid sodium salt (MPTS), an analogue that is not a photoacid, were used to probe differences in proton mobility and local environments in the nanochannels of the three membranes The structures of these fluorescent probes are shown in Figure 2. HPTS

has a pKa of 7.7 in the ground electronic state. Upon excitation to the first electronic excited state, the pKa value drops ~7 units, meaning the conjugate base of HPTS is heavily favored.[28-30] As a result, the proton is ejected and forms a contact ion pair.[28-30] The contact ion pair becomes solvent separated within a few hundred picoseconds.[28-30] Following the ejection of the proton, the deprotonated state of HPTS is left in its excited state.[28-30] Deprotonated HPTS fluoresces at a band center wavelength of 515 nm while the protonated state fluoresces at a band center wavelength of 440 nm. The overwhelming majority of the deprotonated excited state population of HPTS will not undergo recombination with a proton. However, following proton transfer, a small fraction of the deprotonated HPTS will recombine with a proton to reform the protonated state. Dissociation and recombination produces a small population of the protonated state at times very long compared to the initial solvent separation. Deprotonation will again occur followed by solvent separation. As time increases, the probability recombination decreases as the proton formed by dissociation escapes further and further away from the excited deprotonated HPTS. The long time decay (>0.5 ns) of the protonated state population, which is monitored by the protonated state time dependent fluorescence, is related to the rate of proton transfer.[31] Thus, proton mobility in solution plays a large role in the protonated state long time fluorescence decay, making photoacids useful for measuring local proton mobility in the specific membranes.

MPTS is not a photoacid, and fluoresces in a single band. In the ground state, the structures of MPTS and HPTS are almost the same (see Figure 2). The orientational dynamics of MPTS within the membranes were used to understand where HPTS is likely to locate within each nanoconfined system. With such structural similarity, it is highly unlikely that these two probes will locate in different environments in the membrane. By observing the fluorescence

anisotropy decay, the orientational relaxation of MPTS is determined and compared to MPTS orientational relaxation in bulk water. These HPTS and MPTS have been used to study proton mobility in a variety of bulk and confined chemical systems.[32-36]

The proton mobility experiments are sensitive to differences in the hydrogen bonding network found in the regions surrounding the molecule.[37-40] However, for membranes it becomes possible to tune the environment of the fluorescent probes by keeping the fluorinated Teflon backbone the same and varying the pendant chains. It is also possible to change the number density of sulfonate head groups in the channels surrounding the probe through modification of the equivalent weight of the membrane.[41-44] Here we investigated the influences of differences in pendant chain chemical structure and sulfonate head group number density by inserting HPTS and MPTS into 3 membranes: Nafion, 3MB, and 3MC. Orientational dynamics and excited state population decays were studied using MPTS to establish the local environments of the fluorescent probes within each membrane. HPTS was used to investigate proton transfer in each membrane. The experiments were conducted at room temperature and at full hydration. To be able to observe recombination by protons generated via excitation of the HPTS, the sulfonic acid head groups had the hydrogen counterions exchanged for sodium counterions.

Previous experiments have been performed utilizing HTPS in fuel cell membranes to better understand proton transfer dynamics in confined systems.[33, 45] Most notably, a study in which the proton transfer dynamics in Nafion were measured as a function of hydration level, λ, and the results were compared to the proton transfer dynamics in AOT reverse micelles of varying size. These experiments observed a fluorescence decay of the protonated HPTs fluorescence peak at long times that was described using a power law to reflect the recombination of a proton with the deprotonated HPTS. The experiments also

supplied information that estimated the size of the aqueous water domains in Nafion membranes. Here we extend the previous work by comparing Nafion to two other membranes that have different pendant chains and equivalent weights. The experiments are conducted with the membranes fully hydrated. The results again observe recombination dynamics that involve power laws. It is found that the power law exponents, which reflect the facility of proton transport, differ for the three membranes.

II. Materials and Methods

The time correlated single photon counting (TCSPC) technique was used to conduct the fluorescence anisotropy and population decay experiments. The excitation source was a Ti:Sapphire oscillator, which produced ~100 fs laser pulses at a wavelength of 790 nm for orientational relaxation measurements and 760 nm for proton transfer measurements . This wavelength was frequency doubled in a barium borate crystal to 395 nm and 380 nm for excitation of the fluorescent probes. An acousto-optic modulator was used as a single pulse selector to reduce the laser repetition rate from 80 MHz to 5 MHz. A half wave plate mounted in a computer controlled rotation stage was used to rotate the polarization of the excitation beam relative to a fixed polarizer mounted on the entrance slit of a monochromator. The sample was excited from the front surface in an essentially normal geometry through a hole in the lens that collected the fluorescence. A second lens imaged the fluorescence onto the monochromator entrance slit. The collected fluorescence was frequency resolved by a monochromator and single photons were detected with a multichannel plate detector (MCP) at wavelengths ranging from 440 nm to 515 nm.

The instrument response was obtained by measuring the fluorescence of aqueous acidified malachite green with an optical density matching that of the sample, under identical

experimental conditions to the sample measurements. Malachite green has an extremely short fluorescence lifetime, 5 ps, which is short compared to the instrument response, so a measurement of its fluorescence gives the instrument response including the effects of the finite thickness of the sample cell.[46] The instrument response was found to be no more than 85 ps FWHM.

Nafion 117 samples were purchased from fuelcellstore.com. 3M membranes were acquired from Dr. Thomas Zawodzinski at the University of Tennessee – Knoxville. The fluorescent probes 8-hydroxypyrene-1,3,6-trisulfonic acid trisodium salt (HPTS) and . 8-methoxypyrene-1,3,6-trisulfonic acid trisodium salt (MPTS) were purchased from Sigma Aldrich. It was found that several of the membranes contained fluorescent contaminants which absorbed at 395 nm and 380 nm and emitted across the range of interest contributing to the fluorescence decays at all wavelengths. Attempts to characterize the contaminant suggested that it was not uniformly distributed throughout the membrane and may not have been limited to a single compound. This eliminated the possibility of a direct subtraction using a reference sample without the probe, meaning that embedded fluorophores had to be addressed.

To remove the fluorescent impurities, the membranes were refluxed in pure sulfuric acid for 24 hours followed by a reflux in 30% hydrogen peroxide solution. This process was repeated until there was no evidence of fluorescence at the excitation wavelength. TCSPC experiments were conducted on a membrane with negligible fluorescent impurities in order to verify that the membranes were not altered by the sulfuric acid or peroxide washes. Fluorescence decays of treated membranes were similar to those of untreated membranes. Once the background fluorescence was removed, the membranes were refluxed in a 1M NaCl solution for 24 hours to ensure that all protons within the membrane were exchanged for sodium ions. Finally, the

membranes were refluxed in a 0.01M solution of the desired fluorescent probe (HPTS or MPTS) for 24 hours. **Once prepared, samples were stored in scintillation vials in the 0.01M solution of the appropriate probe. It was determined that the concentration of HPTS in the membranes is 4.4 x 10^{-5} M. This value was obtained by quantitatively comparing the absorption spectrum of HPTS in Nafion to those of a series of concentrations of HPTS in bulk water. It was determined that water accounts for 10% of the mass of Nafion in a fully hydrated membrane. This result and the bulk water concentration study provided the necessary information to determine the concentration in Nafion. The fluorescence intensity in the other two membranes is very similar to that of Nafion, which indicates that the concentration of HPTS in all three membranes is very small. The low HPS concentration in the membranes indicates the presence of HPTS will not change the overall structure of the membranes and that HPTS-HPTS interactions are negligible.**

To perform fluorescence experiments, the sample was removed from its scintillation vial and rinsed with distilled water to remove trace amounts of bulk probe solution from the surface of the membrane. The membrane was then sandwiched between two microscope slides and taped around the edges. The absence of birefringence was verified by placing the sample between crossed polarizers. Fluorescence steady state spectra were taken on a Fluorolog-3 fluorescence spectrometer before conducting TCSPC experiments to ensure the purity of the sample. Anisotropy decays of MPTS samples used 395 nm excitation and 440 nm detection. A half wave plate allowed the polarization of the excitation beam to be rotated referenced to a fixed polarizer in front of the entrance slit of the monochromator establishing parallel, perpendicular, and magic angle polarization decays. Population decays of HPTS samples used 380 nm excitation with detection at 440 nm, 450 nm, 460 nm, and 515 nm. In this case, a Glan-Thompson polarizer in

the excitation bean just prior to the sample was fixed at the magic angle relative the fixed polarizer in front of the entrance slit of the monochromator.

To prevent possible photodecomposition of the chromophores from repeated excitation, the sample was slowly moved. The sample was mounted on a motorized computer controlled translation stage. As the data were collected, the sample was slowly translated across its width, back and forth. No appreciable reduction in total fluorescence intensity was detected in the course of the experiments. As a test, data taken at the beginning of an experiment and at the end of an experiment were compared, and they were identical within the noise of the measurement. The repetition rate was also reduced, and it did not change the data.

III. Results and Discussion

A. Lifetimes and Orientational Dynamics

The time-dependent fluorescence anisotropy of the fluorescent probe MPTS was measured to obtain information on its orientational dynamics. Fluorescence anisotropy is measured by collecting intensity decays with polarizations parallel, $I_{\|}(t)$, and perpendicular, $I_{\perp}(t)$, to the excitation polarization. These decays are given by:

$$I_{\|}(t) = P(t)(1 + 0.8C_2(t)) \tag{1}$$

$$I_{\perp}(t) = P(t)(1 - 0.4C_2(t)). \tag{2}$$

$P(t)$ is the excited state population decay and $C_2(t)$ is the 2nd order Legendre polynomial orientational correlation function. $P(t)$ and $C_2(t)$ are expressed as functions of $I_{\|}(t)$ and $I_{\perp}(t)$ and show the relationship between $C_2(t)$ and the fluorescence anisotropy $r(t)$.

$$r(t) = \frac{I_{\|}(t) - I_{\perp}}{I_{\|}(t) + 2I_{\perp}} \tag{3}$$

$$P(t) = \frac{1}{3}(I_{\parallel}(t) + 2I_{\perp}(t)) \quad (4)$$

with

$$r(t) = 0.4C_2(t). \quad (5)$$

Therefore, $r(t)$ reports solely on orientational relaxation with the population decay removed.[47-48] $r(0)$ for fluorescent probes are consistently less than the maximum value of 0.4, a result of ultrafast inertial orientational relaxation.[49] In these samples, $r(0)$ typically has a value of roughly 0.3.

Before examining anisotropy decays, first the population decays, $P(t)$, are analyzed to assign a proper physical interpretation to the data. In bulk water, $P(t)$ is a single exponential. However, it was determined that the MPTS population decays fit well to biexponentials for all three membranes. Figure 3 display the population decays for bulk water and the three membranes, and the decay time constants are given in Table 2. In Figure 3, the bulk water data and the fit can be seen as distinct from the others samples. The data and fits for the three membranes as so similar that they cannot be distinguished in the plot. The membrane data were fit exceptionally well by a biexponential function. A triexponential was tried, and the Akaike Information Criterion (AIC) was used as a statistical test to determine whether a possible increased quality of fit justified the use of a more complex model. When applied to the population decays of MPTS for any of the membranes, the AIC heavily favored a biexponential fits to the data. Within the very small fitting error, values given in Table 2 for the three membranes are identical. All of the membranes have a bulk-like population decay of MPTS with a fluorescence lifetime of ~3.95 ns compared to 4.03 ns of for bulk water. The membrane values are almost within the error bars of the bulk water time constant. In addition to this bulk water like component, they also exhibit another population of MPTS with a lifetime for all three being

the same within experimental error, 2.6 ns. The fast component is 10% of the total decay for the three membranes within error. The population that gives rise to the fast component is probably interaction to some extent with the interface of the nanochannels rather than being more centrally located in the water pool.

Orientational dynamics were extracted from the anisotropy experiments shown in figure 4. Fits to all anisotropy data began at 200 ps to avoid distortions from the instrument response and were taken to times long after total randomization had clearly been achieved. The first 4 ns of the data are shown in Figure 4. As in the population decays, biexponentials were observed for all membranes in contrast to MPTS in bulk water, which has a single exponential anisotropy decay. The procedure for extracting the orientational relaxation in a two component system in which the two components have different lifetimes was used.[40, 50] From the population decays demonstrate that two distinct populations of MPTS exist at a 10:1 ratio. By fixing the relative amplitudes of a biexponential anisotropy fits using the population decay amplitudes and using the two lifetimes, the orientational relaxation time constants of each population were extracted from the anisotropy data. A bulk-like orientational relaxation time constant was found in MPTS in each of the membranes that was, within experimental error, equal to the bulk relaxation time of 130 ps. Therefore, in the fitting, the time constant of the fast component was fixed at 130 ps. The second component has time constants ranging from 400- 650 ps depending on the membrane. The orientational relaxation time constants are given in Table 2. A slower orientational relaxation time constant is consistent with a portion of the probe interacting to some extent with the walls of the membrane. The 3MC membrane trace clearly contains an offset of 0.006. An offset indicates that there is a component of the orientational relaxation that is too slow to measure within the time window set by the fluorescence lifetime. This component is

likely a result of a small subpopulation of MPTS directly associated with the wall of the membrane. This small offset accounts for 2% of the original value of $r(0)$.

Both the population decays, and the orientational relaxation demonstrate that a large majority of the MPTS is in similar environments in all three membranes despite the differences in pendant chain type and equivalent weight of the PEM membrane itself. This finding is not surprising given the size of the probe is relatively small compared the diameter of the fully hydrated membrane pore in which it is confined. The differences in the small slow component of the anisotropy decay may be related to differences in the pendant chain structure and density. Given the structural similarity of MPTS and HPTS, these experiments serve as a good indicator that HPTS molecules will be in very similar environments in the three membranes studies. Then differences in the excited state population decay of HPTS can be attributed to differences in proton transfer.

B. Proton Transfer Dynamics

1. Theoretical Background

In the ground state HPTS has a pKa value of 7.8; however in the first excited state, this value drops to 0.5. The deprotonation and solvent separation time for HPTS is ~90 ps.[28] he remaining non-negligible protonated HTPS population persists for several nanoseconds due to recombination of a dissociated proton with the HTPS conjugate base, a process known as geminate recombination. Here geminate recombination means recombination with a proton that is the result of photo-induced proton dissociation. This long lived population of the protonated state is explicated by the solution to the Smoluchowski equation with electrostatic and back-reaction boundary conditions commonly used to model geminate recombination.[31, 51-52] The

excited state population decay of a photoacid at long time contains a protonated probability term given by[53-54]

$$B(t) \propto \frac{k_{eq}}{(4\pi Dt)^{n/2}} \tag{6}$$

where k_{eq} is the proton transfer equilibrium constant, D is the diffusion coefficient of the proton with HPTS conjugate base effectively stationary in contrast and n is the dimension of the system. With $B(t)$ combined with the excited state population decay, the complete expression of $P(t)$ becomes:

$$P(t) = Ae^{-t/\tau_f} t^{-n/2} \tag{7}$$

where τ_f is the fluorescence lifetime of the photoacid. $n = 3$ for an isotropic three dimensional system where A represents an amplitude term and contains all non-time dependent terms in $B(t)$.

2. Bulk Water

Given the above, a protonated peak of a photoacid in bulk water at long time (>0.5 ns) should decay as $t^{-3/2}$ power law time the excited state lifetime term. This was observed using time resolved fluorescence measurements,[31, 33, 54] and recently additional very detailed experiments were performed to confirm the $t^{-3/2}$ power law.[55] Several sets of experiments were conducted and power law exponents of –1.5 and –1.4 were reported.[55] A recent prior report gave an exponent of –1.1, but this study did not properly account for a small tail of the large deprotonated fluorescence band that runs under the **much smaller protonated band**.[34]

Here, HPTS in bulk water experiments were performed and analyzed to establish a robust procedure to be used in the data analysis of HPTS in the fuel cell membrane nanoconfined systems. In Figure 5, excited state population decays nominally of the protonated band of 10^{-5} M HPTS in bulk water are given across a variety of wavelengths ranging from 460 nm to 490 nm.

To account for both the protonated fluorescence and the fluorescence from the tail of the deprotonated band, data were taken at the several wavelengths shown in Figure 5. By changing the wavelength, the contribution from the deprotonated band changes. The lifetime and the power law exponent, α, should be independent of wavelength, with only the amplitudes of the protonated and deprotonated contributions changing with wavelength. All of the data in Figure 5 were fit to the form

$$P(t) = e^{-t/\tau_f}\,(A_p t^{-\alpha} + A_{dp})\,, \qquad (8)$$

where τ_f, the fluorescent lifetime, was fixed to be 5.4 ns; A_p and A_{dp} are the relative amplitudes of the protonated and deprotonated HPTS populations, respectively. α is the proton transfer exponent, which was allowed to float, but was shared across all wavelengths. The fits in Figure 5 are excellent and yield the proton transfer exponent, $\alpha = 1.39$, a value that agrees with the report by Simkovitch et al. in their most recent publication.[55] A detailed explanation of geminate recombination for HTPS in bulk water is given in that paper.[55]

3. Proton Transfer in Membranes

Steady state fluorescence spectra were taken of HPTS in each of the membranes as well as in bulk water. The normalized spectra are shown in figure 6. The inset is a blow up of the protonated band. In all of the samples, the deprotonated HPTS band is substantially larger than the protonated band in the steady state fluorescence spectra. Upon inspection of the protonated peak, it can be seen that the relative size varies to some extent for the three membranes. Table 3 shows the size of the protonated peak relative to the deprotonated peak of HPTS. 3MB and Nafion membranes have a larger protonated HPTS population than the 3MC membrane where the steady state spectrum behaves much more like bulk water.

In the analysis of the bulk water data, it was assumed that the protonated and deprotonated HTPS populations decay to the ground state with the same lifetimes.[31, 55] This assumption led to the excellent fits shown in Figure 5 for bulk water. The same assumption was made here for the confined systems. The deprotonated state time dependent fluorescence was measure at 515 nm for all the membranes, a wavelength with negligible protonated population, to determine τ_f and to see how similar it is to the 5.4 ns for HPTS in bulk water. The decays are shown in Figure 7. The lifetimes are given in Table 4. The lifetimes range from 5.3 ns to 5.4 ns, all nearly identical to the value for bulk water.

The deprotonated peak decays were fit exceptionally well as single exponentials, in contrast to the results found for MPTS, which required a biexponential to fit the population decay data. The biexponential population decays of MPTS in these confined systems were explained in terms of two ensembles. The major ensemble has the MPTS located near the center of the channels because the major components of the data (lifetime and orientational relaxation) were essentially identical to the bulk water data. The slower component, roughly 10% of the total decay, was assigned to an ensemble of MPTS molecules interacting with the channel wall. These findings were reflected in the fluorescence anisotropy of MPTS in each of the membranes: a biexponential fit with the same amplitude ratio as the population decays with a significant bulk-like reorientation time and smaller component reorienting more slowly, consistent with what one would expect if the MPTS was interacting with the wall of the channel. **The anisotropy of the deprotonated state of HPTS in Nafion was also measured at 515 nm. These data fit to a single exponential with a decay constant of 0.171 ns, very close to the bulk water anisotropy decay. The single exponential lifetime decay (see Figure 7) also indicates the vast majority of the HPTS are in same environments. However, the fit to the**

anisotropy data requires a small long time offset, ~0.01. If the small offset is real, it indicates that there is a fraction of the HPTS that is in a distinct environment that does not permit orientational relaxation. This environment restricts orientational relaxation but is not sufficiently different to make a detectable change the lifetime. There is a broad distribution of channel diameters. It is possible that some of the HPTS is lodged in very narrow channels that inhibit orientational relaxation on the time scale of the measurements.

In the ground state, MPTS and HPTS have very similar structures, both have a –3 negative charge. The only difference in the ground state is that HPTS has a hydroxyl group while MPTS has a methoxy group. One possible explanation for the difference in the fluorescence lifetime decays, biexponential for MPTS but single exponential for HPTS, is that the two molecules differ in charge in the excited state. Proton dissociation from HPTS occurs in a few picoseconds and the contact ion pair is separated in ~100 ps. On times longer than 100 ps, HPTS has a charge of –4. Only ~10% of the MPTS population interacts with the interface, suggesting that the interaction is not attractive and likely repulsive. Once HPTS develops the –4 charge, its repulsion from the wall may increase, forcing the wall-interacting population away from the nanochannel interface. As a simple plausibility test using the Stokes-Einstein equation with the radius of HPTS and the viscosity of bulk water, a molecule near the wall can diffuse 0.5 nm in 125 ps or 1 nm in 500 ps. Data acquisition begins at 500 ps. If the fourth negative charge on HPTS causes a small population near the wall to move toward the channel center, there is sufficient time following excitation but prior to the beginning of the lifetime measurement for the wall interacting ensemble observed for MPTS to vanish.

Equation 8 was used to fit the HPTS protonated band population decays including the small but important contribution from the tail of the deprotonated band. As with the bulk water, the data were fit at several wavelengths to confirm the applicability of Equation 8. The wavelengths 440 nm, 450 nm, and 460 nm were selected for all membranes. In a similar fashion to the bulk water fits, τ_f was fixed to 5.4 and α, the power law exponent, was shared across all wavelengths but allowed to float in value. Sample fits for the membranes and bulk water are shown in Figure 8 at the wavelength 440 nm. As can be seen in the figure, the fits reproduce the data exceedingly well over more than two decades of amplitude decay. The parameters obtained from the fits are given in table 4. At 440 nm, the deprotonated band's 5.4 ns single exponential decay contributes ~10% of the decay amplitude in all samples.

The power law decay form given in Equation 7 with $n = 3$ for an isotropic three dimensional system, yielding a theoretical power law decay term of $t^{-1.5}$, has a detailed theoretical underpinning. Here we are using the same functional form employed to fit the bulk water data (Equation 8) to obtain the power law exponent for comparison among the three membranes and to bulk water. The fits shown in Figure 8 are of high quality, and similar qualities of fits were observed for all wavelengths studied for all membranes, which provides an operational validation of the functional form. While it might be tempting to assign exponents of approximately –0.5 or –1 as reflecting a one dimensional or two dimensional system, respectively, all of the membranes have complex topography nanochannels that cannot reasonably be considered to be one or two dimensional. Rather we take the exponent to be an indicator of the ability of a proton to migrate away from its point of origin. A larger exponent α implies more efficient transfer ability.

From the values of α in Table 4, it can be seen that the 3M membranes have proton transfer that more readily moves the proton away for its initial location than Nafion. Nafion has an α value of 0.55, significantly lower than the 3M membranes with values of 0.93 and 1.05 for 3MB and 3MC, respectively. For all three membranes, the exponents demonstrate that the local proton transfer is more restricted than it is in bulk water. The results indicate that the chemical differences in the Nafion vs. the 3M membranes have a significant influence on proton transfer. Different pendant chains could influence the topography of the channels as well as the hydrogen bond dynamics of the water. As proton transfer involves water hydrogen bond rearrangements, hydrogen bond dynamics can have a substantial effect on proton mobility. In accord with the possibility that the different pendant chains change the hydrogen bond dynamics, simulations performed by Tse and Voth found the room temperature self-diffusion coefficient of water to be higher in 3M membranes compared to the Nafion membrane.[14]

It has been suggested that Nafion pendant chains, due to their extra ether linkage, bend into the water pool forming complexes with the surrounding molecules.[56] In contrast, 3M membranes were seen to be more rigid with the absence of the ether linkage and shorter pendant chains. It has been argued that protons, at least in part, pass along the solvation shells of the sulfonate head groups. Therefore, it is possible that the differences in α values are a result of distinct channel wall structures of Nafion vs. the 3M membranes.[57] In addition to the changes to the hydrogen bond network, significant morphological changes to the pores likely play a significant role in the differences in the observed dynamical information. Simulations have demonstrated the dramatic impact pore shape, even with identical pendant chains, has on overall proton conductivity.[58] Although the photoacids are mainly located away from the channel wall, the proton released upon

photoexcitation should sample all environments, that is, the channel center as well as the water/channel interfaces as indicated by the bulk water diffusion constant, ~9 nm^2/ns[59-60] On the time scale of the experiment, a proton in bulk water will have an rms displacement of ~30 nm. The membrane channels have radii of ~1.5 to ~3.5 nm.[8, 12, 61] While proton diffusion in the membrane channels will be slower than in bulk water, there should be sufficient time for protons to sample all environments, wall and channel center, prior to recombination with the deprotonated photoacid. Therefore, all structural aspects of the channels can contribute to the distinct α values observed for the 3M and Nafion membranes.

While the difference between Nafion and the 3M membranes in the α parameters indicating that efficacy of proton transfer is large, there is only a small difference of ~0.1 in the α values of the 3MB and 3MC membranes. This difference may suggest that changing the number density of sulfonate head groups has some effect on the water in the nanochannels. 3MC has a larger α value and a larger equivalent weight (see Table 1), that is fewer sulfonate head groups per polymer length. However, there have been some studies on the macroscopic behavior of membranes that suggest a smaller equivalent weight is preferable.[13, 62-63] It has been shown that multiple proton mobility mechanisms contribute to the overall proton transport ability of a fuel cell membrane.[64-65] The most efficient manner in which protons diffuse is through the Grotthuss mechanism as is true for bulk water.[64-66] In addition to this mechanism, proton hopping at the interface between water and the negatively charged head groups that line the wall of the channel as well as the mass diffusion of the water molecules can contribute to proton mobility.[64-65, 67] Also of note, the 3MC membrane has a steady state spectrum that is most like that of bulk water, and it also has the proton transfer exponent, α, that is closest to that of bulk water. These results

indicate that water in 3MC membrane nanochannels when swelled to saturation is most like bulk water compared to water in 3MB or Nafion channels.

IV. Concluding Remarks

Time resolved fluorescence experiments were conducted on the photoacid 8-hydroxypyrene-1,3,6-trisulfonic acid sodium salt (HPTS) and a non-photoacid structural analog 8-methoxypyrene-1,3,6-trisulfonic acid sodium salt (MPTS). Both probes were independently inserted into fuel cell membranes Nafion (Dupont), 3MB, and 3MC. Excited state population decays were collected for HPTS to study proton transfer whereas excited state population decays and anisotropy decays were collected for MPTS to better characterize the environment of these molecular probes within the confined water nanochannels of the membranes.

In bulk water it is well established that at long time (>0.5 ns) the decay of the HPTS protonated band fluorescence has the form of a power law times the lifetime exponential decay. The power law is the result of recombination of the HPTS with a proton that was the result of the photoacid proton dissociate following excitation. The power law exponent for bulk water, i.e., an isotropic 3D system, is theoretically predicted to be –1.5 and it was found from experiments to be approximately –1.5. In the nanochannels of the three membranes that were studied, again a power law times the lifetime exponential describes the experimental decays exceedingly well. However, the exponents, $-\alpha$, are all less than –1.5. The size of α was taken to be a measure of the efficacy of proton mobility away from the initially excited photoacid. While Nafion has an α of ~0.5, the 3M membranes have exponents of ~1, indicating that on a nanoscopic distance scale, proton transfer is enhanced in the 3M membranes relative to Nafion. The difference between the two 3M membranes is relatively small, but with 3MC has a larger α by ~0.1, suggesting that is a better proton transport system.

All of the experiments were conducted at room temperature. In practice, fuel cells operate at elevated temperatures, ~100 °C. Future experiments will compare the proton transfer in the three membranes at high temperatures. **Because proton transfer depends on water hydrogen bond rearrangements, and these studies have shown subdiffusive proton transport dynamics,[68] experiments using ultrafast IR methods will be use to directly compare the water dynamics in the three membranes.[33, 40, 50]**

Acknowledgements

We would like to thank Thomas Zawodzinski, Department of Chemical and Biomolecular Engineering, University of Tennessee – Knoxville, for helpful conversations and providing the 3M membranes used in these experiments. This work was funded by the Division of Chemical Sciences, Geosciences, and Biosciences, Office of Basic Energy Sciences of the U.S. Department of Energy through Grant # DE-FG03-84ER13251, (C.M.L. and M.D.F.) and by the Division of Chemistry, Directorate of Mathematical and Physical Sciences, National Science Foundation (NSF) (CHE-1461477) (J.E.T. and M.D.F.). J.E.T. thanks the NSF for a graduate research fellowship. We also thank Patrick Kramer for useful discussions regarding proper data analysis.

References

1. Acres, G. J., Recent Advances in Fuel Cell Technology and Its Applications. *J. Power Sources* **2001,** *100*, 60-66.

2. Kim, J.; Lee, S. M.; Srinivasan, S.; Chamberlin, C. E., Modeling of Proton Exchange Membrane Fuel Cell Performance with an Empirical Equation. *J. Electrochem. Soc.* **1995,** *142*, 2670-2674.

3. Steele, B., Material Science and Engineering: The Enabling Technology for the Commercialisation of Fuel Cell Systems. *J. Mat. Sci.* **2001,** *36*, 1053-1068.

4. Kreutz, T. G.; Ogden, J. M. *Assessment of Hydrogen-Fueled Proton Exchange Membrane Fuel Cells for Distributed Generation and Cogeneration*, Proc. of the 2000 US DOE Hydrogen Prog. Rev., 2000; pp 1-43.

5. Peighambardoust, S. J.; Rowshanzamir, S.; Amjadi, M., Review of the Proton Exchange Membranes for Fuel Cell Applications. *Int. J. Hydrogen Energy* **2010,** *35*, 9349-9384.

6. Dyer, C. K., Fuel Cells for Portable Applications. *J. Power Sources* **2002,** *106*, 31-34.

7. Crabtree, G. W.; Dresselhaus, M. S.; Buchanan, M. V., The Hydrogen Economy. *Physics Today* **2004,** *57*, 39-44.

8. Mauritz, K. A.; Moore, R. B., State of Understanding of Nafion. *Chem. Rev.* **2004,** *104*, 4535-4585.

9. Tsuchiya, H.; Kobayashi, O., Mass Production Cost of PEM Fuel Cell by Learning Curve. *Int. J. Hydrogen Energy* **2004,** *29*, 985-990.

10. Wang, Y.; Chen, K. S.; Mishler, J.; Cho, S. C.; Adroher, X. C., A Review of Polymer Electrolyte Membrane Fuel Cells: Technology, Applications, and Needs on Fundamental Research. *App. Energy* **2011,** *88*, 981-1007.

11. Wee, J.-H., Applications of Proton Exchange Membrane Fuel Cell Systems. *Renew. and Sustain. Eng.Revs.* **2007,** *11*, 1720-1738.

12. Rubatat, L.; Rollet, A. L.; Gebel, G.; Diat, O., Evidence of Elongated Polymeric Aggregates in Nafion. *Macromolecules* **2002,** *35*, 4050-4055.

13. Emery, M.; Frey, M.; Guerra, M.; Haugen, G.; Hintzer, K.; Lochhaas, K. H.; Pham, P.; Pierpont, D.; Schaberg, M.; Thaler, A., The Development of New Membranes for Proton Exchange Membrane Fuel Cells. *ECS Transactions* **2007,** *11*, 3-14.

14. Tse, Y.-L. S.; Herring, A. M.; Kim, K.; Voth, G. A., Molecular Dynamics Simulations of Proton Transport in 3M and Nafion Perfluorosulfonic Acid Membranes. *J. Phys. Chem. C* **2013,** *117*, 8079-8091.

15. Schmidt-Rohr, K.; Chen, Q., Parallel Cylindrical Water Nanochannels in Nafion Fuel-Cell Membranes. *Nat. Mat.* **2008,** *7*, 75-83.

16. Elliott, J. A.; Wu, D.; Paddison, S. J.; Moore, R. B., A Unified Morphological Description of Nafion Membranes from Saxs and Mesoscale Simulations. *Soft Matter* **2011,** *7*, 6820-6827.

17. Roche, E.; Pineri, M.; Duplessix, R.; Levelut, A., Small-Angle Scattering Studies of Nafion Membranes. *J. Polym. Sci.: Polym. Phys. Ed.* **1981,** *19*, 1-11.

18. Rieberer, S.; Norian, K. H., Analytical Electron-Microscopy of Nafion Ion-Exchange Membranes. *Ultramicroscopy* **1992,** *41*, 225-233.

19. Ceynowa, J., Electron-Microscopy Investigation of Ion-Exchange Membranes. *Polymer* **1978,** *19*, 73-76.

20. Xue, T.; Trent, J. S.; Osseo-Asare, K., Charachterization of Nafion Membranes by Transmission Electron-Microscopy. *J. Membr. Sci.* **1989,** *45*, 261-271.

21. Gierke, T. D.; Munn, G. E.; Wilson, F. C., The Morphology in Nafion* Perfluorinated Membrane Products, as Determined by Wide- and Small-Angle X-Ray Studies. *J. Polym. Sci.: Polym. Phys. Ed.* **1981,** *19*, 1687-1704.

22. Hsu, W. Y.; Gierke, T. D., Elastic Theory for Ionic Clustering in Perfluorinated Ionomers. *Macromolecules* **1982,** *15*, 101-105.

23. Gebel, G., Structural Evolution of Water Swollen Perfluorosulfonated Ionomers from Dry Membrane to Solution. *Polymer* **2000,** *41*, 5829-5838.

24. Rubatat, L.; Gebel, G.; Diat, O., Fibrillar Structure of Nafion: Matching Fourier and Real Space Studies of Corresponding Films and Solutions. *Macromolecules* **2004,** *37*, 7772-7783.

25. Falk, M., An Infrared Study of Water in Perfluorosulfonate (Nafion) Membranes. *Canadian J. Chem.* **1980,** *58*, 1495-1501.

26. Blake, N. P.; Petersen, M. K.; Voth, G. A.; Metiu, H., Structure of Hydrated Na-Nafion Polymer Membranes. *J. Phys. Chem. B.* **2005,** *109*, 24244-24253.

27. Jalani, N. H.; Datta, R., The Effect of Equivalent Weight, Temperature, Cationic Forms, Sorbates, and Nanoinorganic Additives on the Sorption Behavior of Nafion®. *J. Mem. Sci.* **2005,** *264*, 167-175.

28. Spry, D. B.; Goun, A.; Fayer, M. D., Identification and Properties of the 1la and 1lb States of Pyranine (HPTS). *J. Chem. Phys.* **2006,** *125*, 144514.

29. Leiderman, P.; Genosar, L.; Huppert, D., Excited-State Proton Transfer: Indication of Three Steps in the Dissociation and Recombination Process. *J. Phys. Chem. A* **2005,** *109*, 5965-5977.

30. Pines, E.; Huppert, D., Geminate Recombination Proton-Transfer Reactions. *Chem. Phys. Lett.* **1986,** *126*, 88-91.

31. Agmon, N.; Pines, E.; Huppert, D., *J. Chem. Phys.* **1988,** *88*, 5631-5639.

32. Spry, D. B.; Goun, A.; Fayer, M. D., Deprotonation Dynamics and Stokes Shift of Pyranine (HPTS). *J. Phys. Chem. A* **2007,** *111*, 230-237.

33. Spry, D. B.; Goun, A.; Glusac, K.; Moilanen, D. E.; Fayer, M. D., Proton Transport and the Water Environment in Nafion Fuel Cell Membranes and AOT Reverse Micelles. *J. Am. Chem. Soc* **2007,** *129*, 8122-8130.

34. Lawler, C.; Fayer, M. D., Proton Transfer in Ionic and Neutral Reverse Micelles. *J. Phys. Chem. B* **2015,** *119*, 6024-6034.

35. Sedgwick, M.; Cole, R. L.; Rithner, C. D.; Crans, D. C.; Levinger, N. E., Correlating Proton Transfer Dynamics to Probe Location in Confined Environments. *J. Am. Chem. Soc.* **2012,** *134*, 11904-11907.

36. Mojumdar, S. S.; Mondal, T.; Das, A. K.; Dey, S.; Bhattacharyya, K., Ultrafast and Ultraslow Proton Transfer of Pyranine in an Ionic Liquid Microemulsion. *J. Chem. Phys.* **2010,** *132*, 194505.

37. Moilanen, D. E.; Fenn, E. E.; Wong, D.; Fayer, M. D., Water Dynamics at the Interface in AOT Reverse Micelles. *J. Phys. Chem. B.* **2009,** *113*, 8560-8568.

38. Fenn, E. E.; Wong, D. B.; Giammanco, C. H.; Fayer, M. D., Dynamics of Water at the Interface in Reverse Micelles: Measurements of Spectral Diffusion with Two-Dimensional Infrared Vibrational Echoes. *J. Phys. Chem. B* **2011,** *115*, 11658-11670.

39. Moilanen, D. E.; Piletic, I. R.; Fayer, M. D., Tracking Water's Response to Structural Changes in Nafion Membranes. *J. Phys. Chem. A.* **2006,** *110*, 9084-9088.

40. Moilanen, D. E.; Piletic, I. R.; Fayer, M. D., Water Dynamics in Nafion Fuel Cell Membranes: The Effects of Confinement and Structural Changes on the Hydrogen Bonding Network. *J. Phys. Chem. C.* **2007,** *111*, 8884-8891.

41. Choi, J.; Lee, K. M.; Wycisk, R.; Pintauro, P. N.; Mather, P. T., Nanofiber Composite Membranes with Low Equivalent Weight Perfluorosulfonic Acid Polymers. *J. Mater. Chem.* **2010,** *20*, 6282-6290.

42. Lei, C.; Bessarabov, D.; Ye, S.; Xie, Z.; Holdcroft, S.; Navessin, T., Low Equivalent Weight Short-Side-Chain Perfluorosulfonic Acid Ionomers in Fuel Cell Cathode Catalyst Layers. *J. Power Sources* **2011,** *196*, 6168-6176.

43. Ezzell, B. R.; Carl, W. P., Low Equivalent Weight Sulfonic Fluoropolymers. Google Patents: 1990.

44. Fontanella, J. J.; Edmondson, C. A.; Wintersgill, M. C.; Wu, Y.; Greenbaum, S. G., High-Pressure Electrical Conductivity and NMR Studies in Variable Equivalent Weight Nafion Membranes. *Macromolecules* **1996,** *29*, 4944-4951.

45. Spry, D.; Fayer, M., Proton Transfer and Proton Concentrations in Protonated Nafion Fuel Cell Membranes. *J. Phys. Chem. B* **2009,** *113*, 10210-10221.

46. Wirth, P.; Schneider, S.; Dörr, F., S 1-Lifetimes of Triphenylmethane and Indigo Dyes Determined by the Two-Photon-Fluorescence Technique. *Opt. Comm.* **1977,** *20*, 155-158.

47. Tao, T., Time-Dependent Fluorescence Depolarization and Brownian Rotational Diffusion Coefficients of Macromolecules. *Biopolymers* **1969,** *8*, 609-632.

48. Tan, H.-S.; Piletic, I. R.; Fayer, M., Polarization Selective Spectroscopy Experiments: Methodology and Pitfalls. *JOSA B* **2005,** *22*, 2009-2017.

49. Xu, J.; Shen, X.; Knutson, J. R., Femtosecond Fluorescence Upconversion Study of the Rotations of Perylene and Tetracene in Hexadecane. *J. Phys. Chem. A* **2003,** *107*, 8383-8387.

50. Moilanen, D. E.; Piletic, I. R.; Fayer, M. D., Tracking Water's Response to Structural Changes in Nafion Membranes. *J. Phys. Chem. A.* **2006,** *110*, 9084-9088.

51. Agmon, N.; Szabo, A., Reversable Diffusion-Influenced Reactions. *J. Chem. Phys.* **1990,** *92*, 5270-5284.

52. Goun, A.; Glusac, K.; Fayer, M. D., Photoinduced Electron Transfer and Geminate Recombination in Liquids on Short Time Scales: Experiments and Theory. *J. Chem. Phys.* **2006,** *124*, 084504.

53. Hong, K. M.; Noolandi, J., Solution of the Smoluchowski Equation with a Coulomb Potential. I. General Results. *J. Chem. Phys.* **1978,** *68*, 5163-5171.

54. Huppert, D.; Goldberg, S. Y.; Masad, A.; Agmon, N., Experimental Determination of the Long-Time Behavior in Reversible Binary Chemical Reactions. *Phys. Rev. Lett.* **1992,** *68*, 3932.

55. Simkovitch, R.; Pines, D.; Agmon, N.; Pines, E.; Huppert, D., Reversible Excited-State Proton Geminate Recombination - Revisited. *J. Phys. Chem. B* **2016,** *120*, 12615-12632.

56. Sunda, A. P.; Venkatnathan, A., Molecular Dynamics Simulations of Side Chain Pendants of Perfluorosulfonic Acid Polymer Electrolyte Membranes. *J. Mat. Chem. A* **2013,** *1*, 557-569.

57. Savage, J.; Tse, Y.-L. S.; Voth, G. A., Proton Transport Mechanism of Perfluorosulfonic Acid Membranes. *J. Phys. Chem. C* **2014,** *118*, 17436-17445.

58. Liu, S.; Savage, J.; Voth, G. A., Mesoscale Study of Proton Transport in Proton Exchange Membranes: Role of Morphology. *J. Phys. Chem. C* **2015,** *119*, 1753-1762.

59. Roberts, N. K.; Northey, H. L., Proton and Deuteron Mobility in Normal and Heavy Water Solutions of Electrolytes. *J. Chem. Soc., Faraday Trans. 1: P. Chem. Con. Phases* **1974,** *70*, 253-262.

60. Agmon, N., The Grotthuss Mechanism. *Chem. Phys. Lett.* **1995,** *244*, 456-462.

61. Liu, Y.; Horan, J. L.; Schlichting, G. J.; Caire, B. R.; Liberatore, M. W.; Hamrock, S. J.; Haugen, G. M.; Yandrasits, M. A.; Seifert, S.; Herring, A. M. A., Small-Angle X-Ray Scattering

Study of the Development of Morphology in Films Formed from the 3M Perfluorinated Sulfonic Acid Ionomer. *Macromolecules* **2012,** *45*, 7495-7503.

62. Maalouf, M.; Pyle, B.; Sun, C.-N.; Wu, D.; Paddison, S. J.; Schaberg, M.; Emery, M.; Lochhaas, K. H.; Hamrock, S. J.; Ghassemi, H., Proton Exchange Membranes for High Temperature Fuel Cells: Equivalent Weight and End Group Effects on Conductivity. *ECS Transactions* **2009,** *25*, 1473-1481.

63. Kreuer, K. D.; Schuster, M.; Obliers, B.; Diat, O.; Traub, U.; Fuchs, A.; Klock, U.; Paddison, S. J.; Maier, J., Short-Side-Chain Proton Conducting Perfluorosulfonic Acid Ionomers: Why They Perform Better in PEM Fuel Cells. *J. Power Sources* **2008,** *178*, 499-509.

64. Choi, P.; Jalani, N. H.; Datta, R., Thermodynamics and Proton Transport in Nafion II. Proton Diffusion Mechanisms and Conductivity. *J. Electrochem. Soc.* **2005,** *152*, E123-E130.

65. Paddison, S. J.; Paul, R., The Nature of Proton Transport in Fully Hydrated Nafion®. *PCCP* **2002,** *4*, 1158-1163.

66. Marx, D.; Tuckerman, M. E.; Hutter, J.; Parrinello, M., The Nature of the Hydrated Excess Proton in Water. *Nature* **1999,** *397*, 601-604.

67. Devanathan, R.; Venkatnathan, A.; Rousseau, R.; Dupuis, M.; Frigato, T.; Gu, W.; Helms, V., Atomistic Simulation of Water Percolation and Proton Hopping in Nafion Fuel Cell Membrane. *J. Phys. Chem. B* **2010,** *114*, 13681-13690.

68. Savage, J.; Voth, G. A., Persistent Subdiffusive Proton Transport in Perfluorosulfonic Acid Membranes. *J. Phys. Chem. Lett.* **2014,** *5*, 3037-3042.

Table 1. Membrane names and properties

Membrane[a]	Full Name[b]	Thickness[c](μm)	Equivalent Weight[d] (amu)	λ (H_2O/SO_3^-)
Nafion	Nafion 117	178	1100	8
3MB	3M-1513232B	50	825	8
3MC	3M-1513231C	50	1000	9

a The shorthand name given to the membrane for the purposes of this paper
b The industrial name of the membrane
c The thickness of the membranes studied in microns
d The equivalent weight of the membranes, or the molecular mass of a polymer segment that contains a single pendant chain with one sulfonate head group.
e The hydration of the membrane in units of water molecules per sulfonate head group

Table 2. MPTS population and anisotropy decay time constants

	Nafion	3MB	3MC	Bulk Water
Equivalent Weight[a]	1100	825	1000	--
Population Decay – Fluorescence Lifetimes				
τ_{f1} (ns)[b]	3.94± 0.010	3.93 ± 0.007	3.97 ± 0.007	4.03± 0.002
τ_{f2} (ns)[b]	2.64 ± 0.12	2.53 ± 0.09	2.63 ± 0.06	--
Anisotropy Decay – Rotational Lifetimes				
τ_{r1} (ns)[c]	0.13	0.13	0.13	0.135 ± 0.012
τ_{r2} (ns)[c]	0.43 ± 0.09	0.50 ± 0.08	0.64 ± 0.09	--

a Molecular mass of one pendant chain and Teflon backbone strand (Figure 1)
b Fluorescence lifetimes found to fits of excited state population decays
c Rotational lifetimes found to fits of anisotropy decays

Table 3. HPTS Protonated peak maximum relative to the deprotonated peak maximum from the steady state spectra in Figure 6 with the deprotonated peak normalized to 1.

	Nafion	3MB	3MC	Bulk Water
protonated peak	0.039	0.043	0.028	0.024

Table 4. HPTS fluorescence lifetimes, amplitudes, and power law exponents

Membrane	τ_f(ns)[a]	A_p[b]	A_{dp}[c]	α[d]
Nafion	5.30±0.003	0.224±0.001	0.0225±0.001	0.55±0.005
3MB	5.4±0.0009	0.104±0.001	0.0115±0.003	0.93±0.007
3MC	5.35±0.0004	0.058±0.001	0.0076±0.001	1.05±0.004
Bulk water	5.39±0.0004	0.060±0.001	0.0057±0.0008	1.39±0.001

a Fluorescence lifetime measured by fitting the population decay of the 515 nm emission near the peak of the deprotonated population. Data shown in Figure 7.
b The amplitude of the protonated population contribution to the fit of Figure 8
c The amplitude of the deprotonated population contribution to the fit of Figure 8
d The proton transfer exponent. Larger numbers indicate more efficient proton migration.

Figure Captions

Figure 1. Repeat structures of Nafion (left) and 3M (right) membrane polymers.

Figure 2. Pyrene derivatives 1-hydroxypyrene-3 6 8-trisulfonic acid (HPTS) and 1-methoxypyrene-3 6 8-trisulfonic acid (MPTS)

Figure 3. Excited state population decays of MPTS in fully hydrated membranes and in bulk water. The membranes' data fit well to biexponential decays with a bulk water component (90%) and a faster component, whereas the data in bulk water fit to a single exponential. The red curves are the corresponding fits.

Figure 4. Anisotropy decays of MPTS in fully hydrated membranes and in bulk water. The membranes data fit well to biexponential decays with a bulk water component (90%) and a slower component, whereas the data in bulk water fit to a single exponential. The red curves are the corresponding fits.

Figure 5. Excited state protonated band population decays of HPTS in bulk water across several wavelengths and fits to the data. The data were fit using Equation 8. The consistency of the fits for the range of wavelengths confirms the efficacy of Equation 8. The red curves are the fits, which obscure the underlying data in most cases.

Figure 6. Steady-state emission spectra of HPTS in bulk water (black), fully hydrated 3MB (purple), fully hydrated 3MC (green), and fully hydrated Nafion (blue). The large bands are from the deprotonated populations. The small bands to the blue are the protonated bands. The inset is a blow up of the protonated bands.

Figure 7. Excited state population decays of the deprotonated HPTS bands collected at 515 nm in all membranes and bulk water. The data fit to a single exponential in all cases.

Figure 8. Excited state population decays HPTS collected at 440 nm for all membranes and bulk water. Each data set was fit using Equation 8 and fit globally at 3 different emission wavelengths, 440 nm, 450 nm, 460 nm, to determine the proton migration exponent, α, a term which was shared in the fits at all emission wavelengths. The red curves are the resulting fits for the 440 nm data.

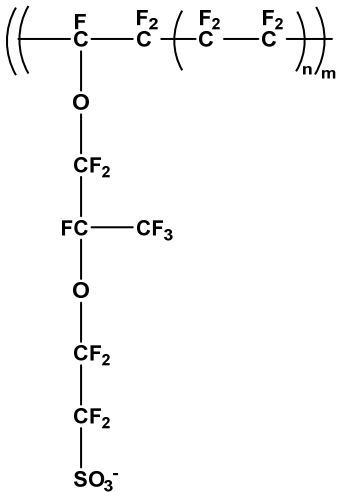

Nafion

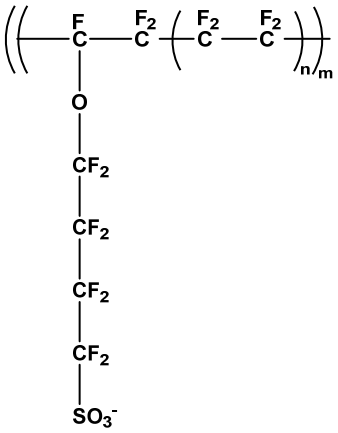

3M

Figure 1

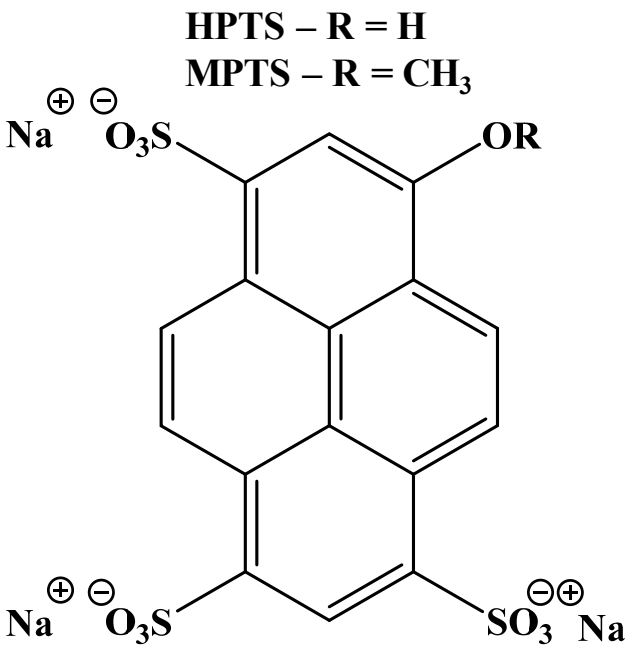

Figure 2

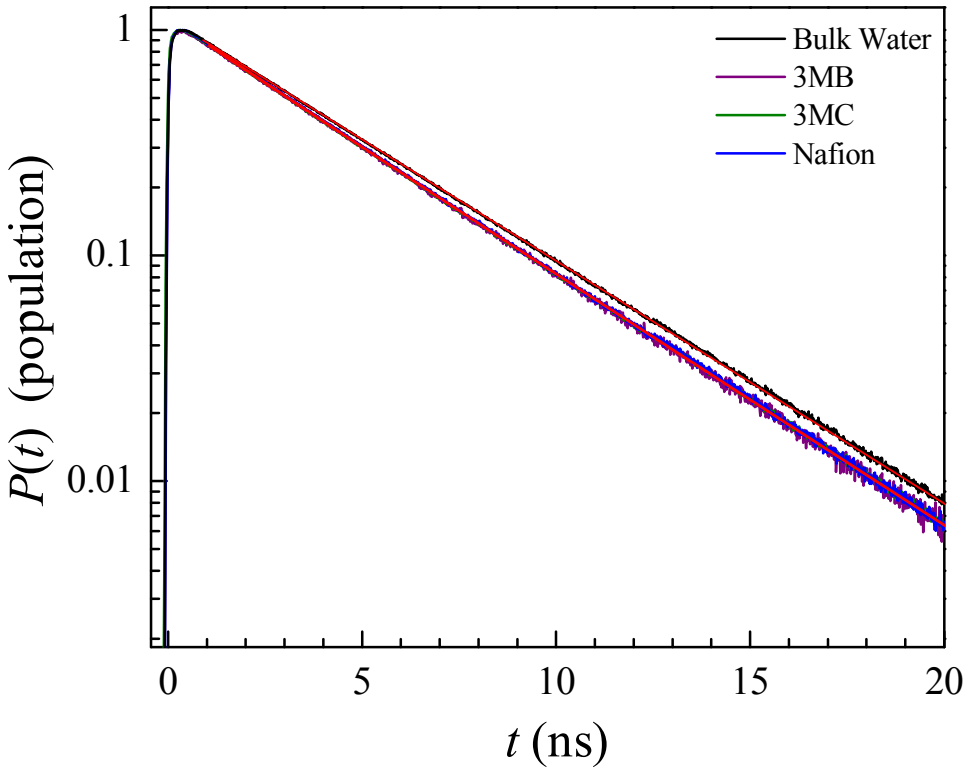
1
0.1
0.01
P(t) (population)
0
5
10
15
20
t (ns)
Bulk Water
3MB
3MC
Nafion

Figure 3

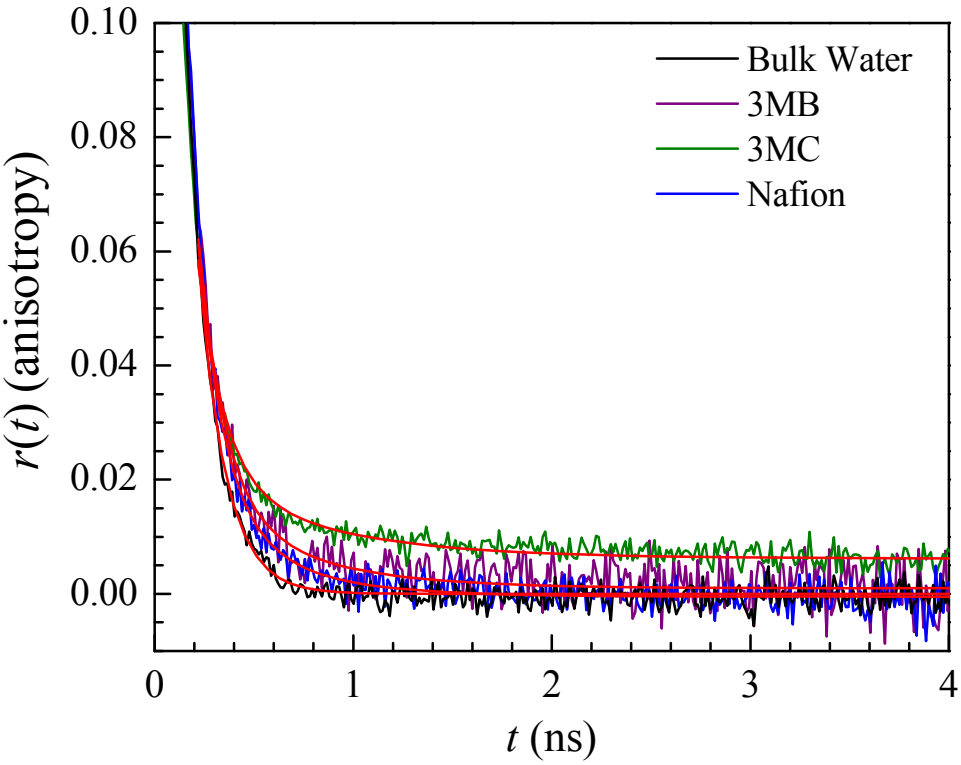
0.10
0.08
0.06
0.04
0.02
0.00
r(t) (anisotropy)
0
1
2
3
4
t (ns)
Bulk Water
3MB
3MC
Nafion

Figure 4

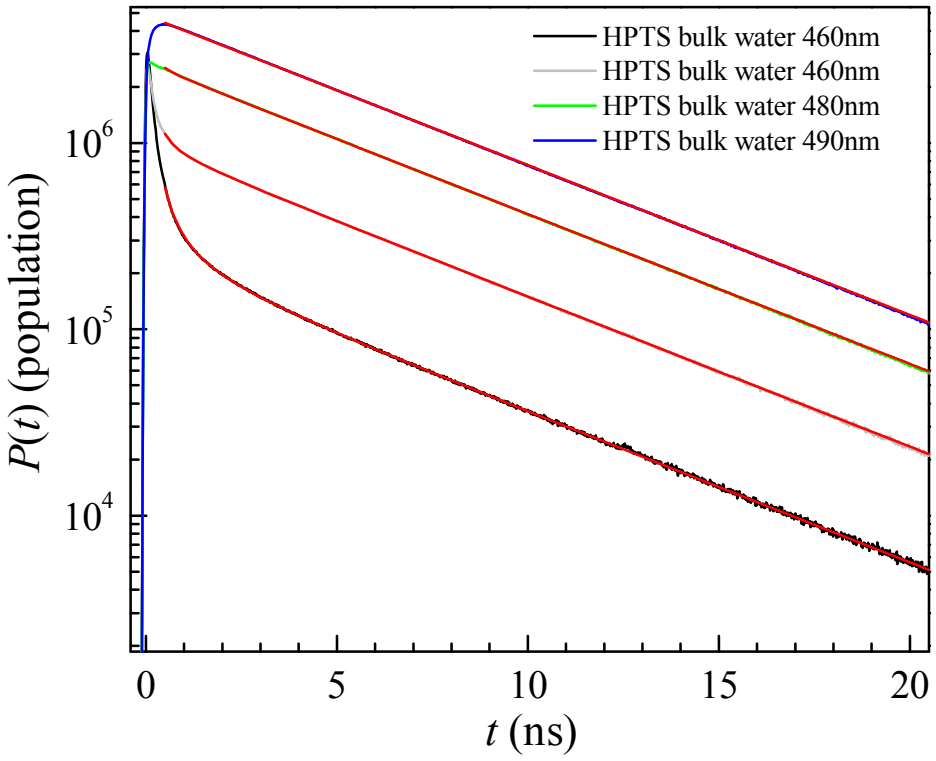
HPTS bulk water 460nm
HPTS bulk water 460nm
HPTS bulk water 480nm
HPTS bulk water 490nm
P(t) (population)
10^6
10^5
10^4
0
5
10
15
20
t (ns)

Figure 5

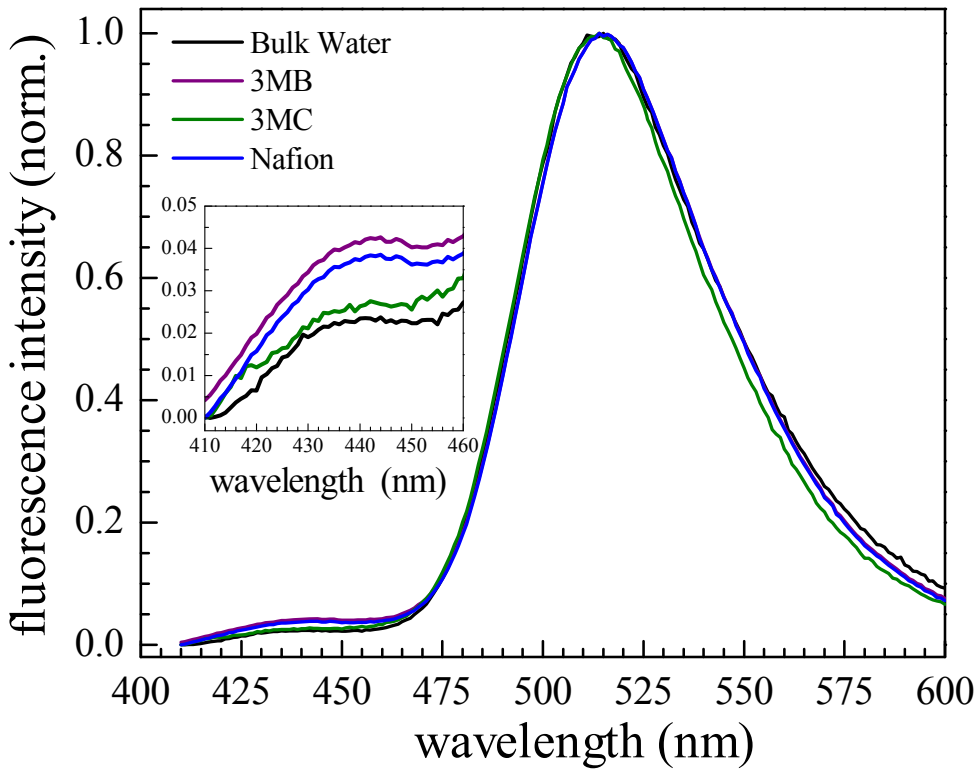
Bulk Water
3MB
3MC
Nafion
fluorescence intensity (norm.)
wavelength (nm)
1.0
0.8
0.6
0.4
0.2
0.0
400
425
450
475
500
525
550
575
600
0.05
0.04
0.03
0.02
0.01
0.00
410
420
430
440
450
460
wavelength (nm)

Figure 6

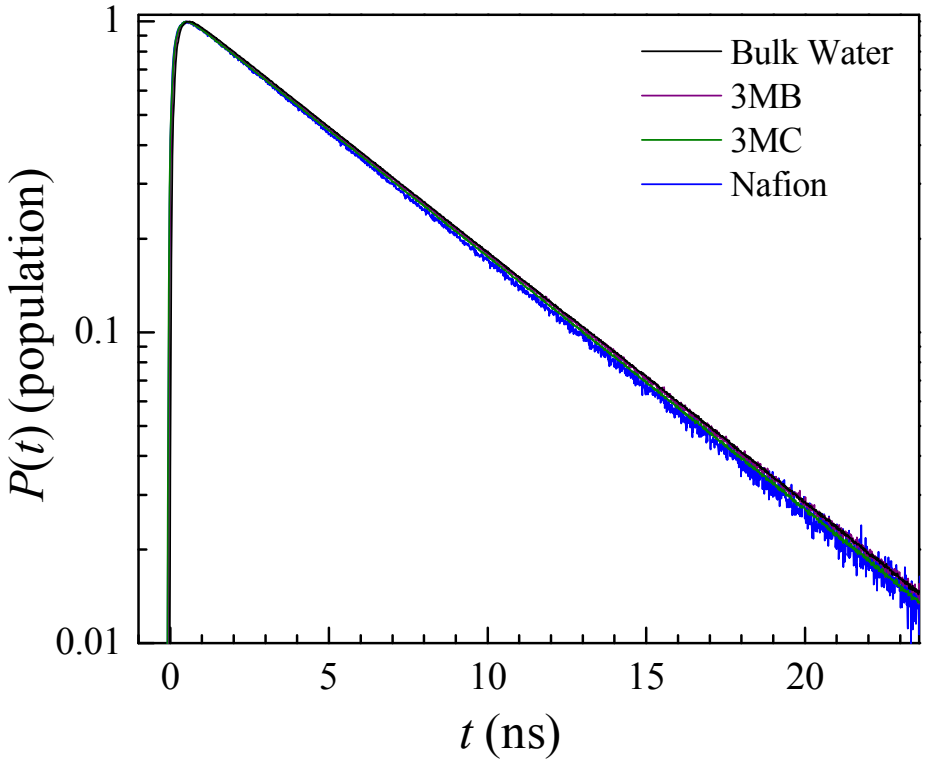
1
0.1
0.01
P(t) (population)
0
5
10
15
20
t (ns)
Bulk Water
3MB
3MC
Nafion

Figure 7

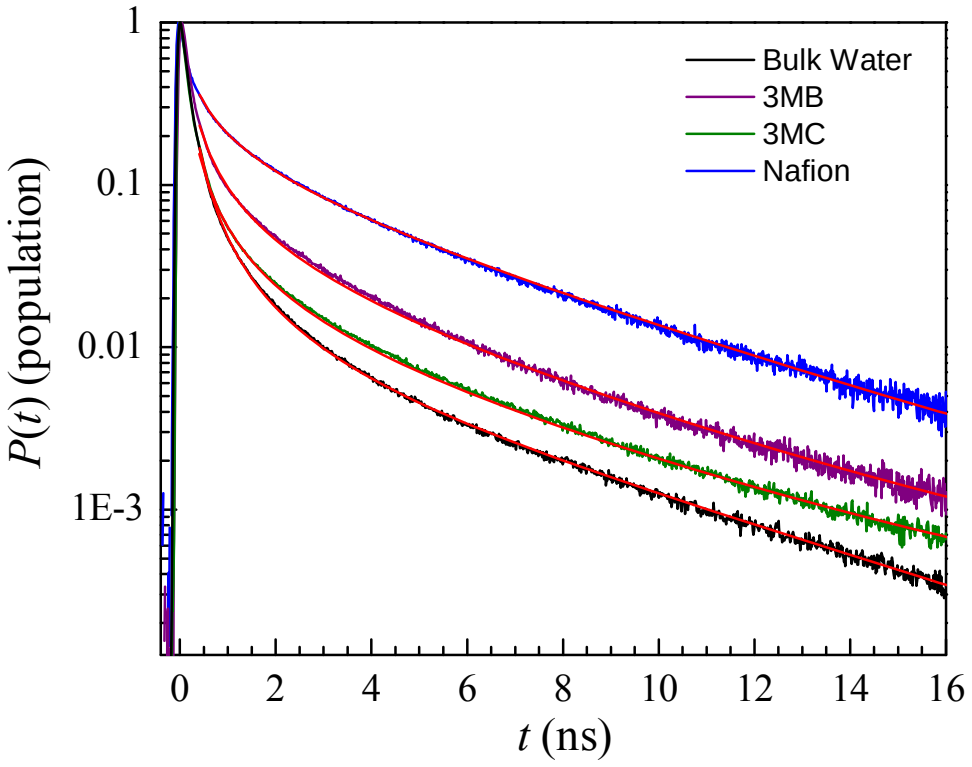
1
0.1
0.01
1E-3
P(t) (population)
0
2
4
6
8
10
12
14
16
t (ns)
Bulk Water
3MB
3MC
Nafion

Figure 8

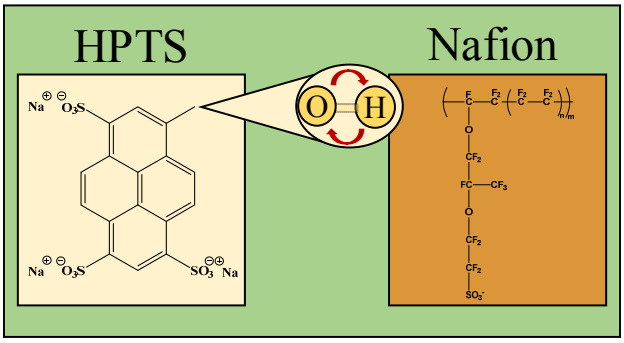

TOC Graphic